



## City Research Online

### City, University of London Institutional Repository

---

**Citation:** Ghosh, S. and Rahman, B. M. (2016). An Innovative Straight Resonator Incorporating a Vertical Slot as an Efficient Bio-Chemical Sensor. IEEE Journal on Selected Topics in Quantum Electronics, 23(2), doi: 10.1109/JSTQE.2016.2630299

This is the accepted version of the paper.

This version of the publication may differ from the final published version.

---

**Permanent repository link:** <https://openaccess.city.ac.uk/id/eprint/16546/>

**Link to published version:** <http://dx.doi.org/10.1109/JSTQE.2016.2630299>

**Copyright:** City Research Online aims to make research outputs of City, University of London available to a wider audience. Copyright and Moral Rights remain with the author(s) and/or copyright holders. URLs from City Research Online may be freely distributed and linked to.

**Reuse:** Copies of full items can be used for personal research or study, educational, or not-for-profit purposes without prior permission or charge. Provided that the authors, title and full bibliographic details are credited, a hyperlink and/or URL is given for the original metadata page and the content is not changed in any way.



## An Innovative Straight Resonator Incorporating a Vertical Slot as an Efficient Bio-Chemical Sensor

Journal:	<i>Journal of Selected Topics in Quantum Electronics</i>
Manuscript ID	JSTQE-CON-PS2017-06432-2016.R2
Manuscript Type:	Contributed
Date Submitted by the Author:	05-Oct-2016
Complete List of Authors:	Ghosh, Souvik; City University, School of Mathematics, Computer Science and Engineering Rahman, B M A; City University London, EEIE; City University London, Electrical & Electronic Engineering
Keyword:	Finite element methods, Integrated optics, Resonators

# An Innovative Straight Resonator Incorporating a Vertical Slot as an Efficient Bio-Chemical Sensor

Souvik Ghosh and B. M. A. Rahman, *Fellow, IEEE*

**Abstract**— A compact and integrated label-free refractometric bio-chemical sensor based on silicon-on-insulator (SOI) is proposed and comprehensively studied at the telecommunication wavelength of  $\lambda = 1550 \text{ nm}$ . This device incorporated a three dimensional (3D) Fabry-Perot cavity in the nano-scale regime with maximum footprint area around  $470 \times 473 \text{ nm}^2$ . A resonance shift ( $\Delta\lambda_{res}$ ) of  $5.2 \text{ nm}$  is reported for an ultra-thin ( $5 \text{ nm}$ ) bio-layer sensing. Besides, an improved maximum sensitivity ( $S = 820 \text{ nm/RIU}$ ) is also achieved for bulk refractive index change in surroundings. As a chemical sensor, very low detection limit ( $DL = 6.1 \times 10^{-6} \text{ RIU}$ ) also can be possible to achieve by this device. All the numerical investigations and optimizations were carried out in frequency domain by a numerically efficient and rigorous full vectorial H-field based two dimensional (2D) and three dimensional (3D) finite element methods (FEM). A 3D-FEM code is developed and used to find out the wavelength dependencies of the resonator. Possibility of easy CMOS fabrication and integration opportunities make this structure as a prospective and efficient lab-on-chip device.

**Index Terms** — Finite Element Method, Integrated Optics, Resonator, Sensors.

## I. INTRODUCTION

Following the initial work by Graham Reed, Richard Soref first proposed the fabrication of silicon waveguides in a silicon-on-insulator (SOI) wafer in the telecom wavelength range,  $1200 - 1600 \text{ nm}$  [1]. The high-refractive-index contrast of SOI structures leads to the higher degree of light confinement and guidance through the silicon layer. This property can make the silicon waveguides and resonators to be the basic building blocks of compact photonic integrated circuits (PIC). Over the last two decades, silicon technology has attracted considerable attentions due to its potential low-cost by exploiting the CMOS fabrication technology, developed for electronics, which can also be used by the photonics industries.

Light confinement in low-index slot section was first reported in 2004 [2] and since then SOI based slot waveguide became an intriguing area of research. The boundary condition

of electromagnetic field demands normal component of electric flux density ( $\mathbf{D}$ ) must be continuous at the dielectric interface, which results a high magnitude electric field ( $\mathbf{E}$ ) discontinuity at the same interface. These characteristics lead to a strong field enhancement in the low-index slot region. As a result, the slot waveguides becoming an attractive choice as a refractive index (RI) based biological and chemical sensors. By combining the slot properties with resonating devices, a higher sensitivity can be achieved. Combination of slot configuration with ring resonator was first investigated and fabricated by Barrios *et al.* [3], [4] on a  $\text{Si}_3\text{N}_4 - \text{SiO}_2$  platform with a maximum sensitivity of  $212 \text{ nm/RIU}$ . An improved sensitivity of  $298 \text{ nm/RIU}$  has also been reported by Claes *et al.* [5] for the similar slot waveguide based ring resonator in SOI platform. These structural devices show significant improvement of refractive index sensitivity over the conventional strip waveguide based ring resonator, demonstrated by K. D. Vos *et al.* [6]. Integration of Bragg gratings on SOI platform with promising application in bio and chemical sensing has also been reported [7], [8]. The conventional strip and rib waveguide based Bragg gratings use the evanescent field tails for the sensing, thus exhibiting a lower sensitivity with high quality (Q) factor. Wang *et al.* recently proposed an improved slot waveguide based Bragg sensors with sensitivity as high as  $340 \text{ nm/RIU}$  around  $1550 \text{ nm}$  wavelength with the help of enhanced light matter interaction into the slotted region [9]. Recently, an improved bulk detection sensitivity ( $380 \text{ nm/RIU}$ ) of porous silicon ring resonator for biosensing applications has been reported by G. A. Rodrigues *et al.* [10]. Other optical bio-chemical sensors have incorporated microdisk resonator [11], photonic crystal cavities [12], [13] and Mach-Zehnder interferometers [14], [15].

In this paper, we present a detailed theoretical and numerical investigations of three dimensional single vertically-slotted resonator structure in a SOI platform. An in-house numerically efficient and rigorous three dimensional full vectorial  $\mathbf{H}$ -field based finite element method (3D-FEM) is developed and used to obtain the modal solutions at the particular resonating wavelength. Initially, optimizations of design parameters, such as the width (W), height (H) and slot width ( $W_s$ ) are carried out by a two dimensional full-vectorial  $\mathbf{H}$ -field based Finite Element Method (2D-FEM). Subsequently the resonating modal fields, sensitivity (S) and detection limit (DL) of this optimized device have been

Souvik Ghosh is with the Department of School of Mathematics, Computer Science and Engineering, City University London, Northampton Square, London, EC1V 0HB, UK (e-mail: souvik.ghosh.1@city.ac.uk).

B. M. A. Rahman is with the Department of School of Mathematics, Computer Science and Engineering, City University London, Northampton Square, London, EC1V 0HB, UK (e-mail: B.M.A.Rahman@city.ac.uk).

calculated by the 3D-FEM. Interestingly, we observed an effective change in sensitivity from 635 nm/RIU to 820 nm/RIU depending on the position of the perfect electric wall (PEW) in the device. As the detection limit (DL) of the sensor device is inversely related to the sensitivity (S), the changes in the sensitivity due to metal boundary position also makes a noticeable change in the detection limit (DL). Such a high sensitivity and detection limit achieved by proposed device can be invaluablely important in the field of chemical sensing. We have validated this phenomenon with sucrose solution at ambient temperature (20°C). It has been noticed that bio-molecules become transparent in the near infrared region (NIR). Hence the dominated optical absorption is governed by the water solvent which shows a dip in the absorption spectrum at 1550 nm wavelength. Hence we selected the operating wavelength of the device for bio-chemical sensing around 1550 nm, the standard telecommunication wavelength, which adds an extra advantage of availability of standardized resources of the telecommunication band to design the nano-structured sensing setup.

This paper is arranged as follows. In 2<sup>nd</sup> section, we first demonstrate a concise mathematical steps of the full vectorial **H**-field based three dimensional finite element method (3D-FEM) for resonating structures. The 3<sup>rd</sup> section gives the description of our proposed structure with its geometrical parameters. In this section, all the design parameters are optimized by numerically accurate 2D-FEM. In 4<sup>th</sup> section, we report the excellent sensing ability of the proposed device as a bio-chemical sensor. The modal responses at the resonating wavelength are obtained by using the 3D-FEM code. Finally, all findings are summarized in the *conclusive* part.

## II. VECTOR FORMULATION OF 3D-FEM

In general, to accomplish the theoretical investigation of a photonic device it is required to solve the partial differential equations (PDEs) and in most cases, the equations under consideration are much complex to be solved by using an analytical or semi-analytical methods. Solutions of Maxwell's equations are the essential part to design and analyze the integrated photonic waveguides and resonators. For the modal solutions of waveguide structures, a full vectorial 2D-FEM has been established as the most efficient approach and our in-house code developed and refined over last 30 years has been very effective [16]-[18]. However, to investigate the three dimensional (3D) optical resonating structures with isotropic

variational expressions can present the propagation constants of the fundamental and higher order quasi-TE and TM modes. On the other hand, for the 3D resonating structures, variational expression calculates the resonant frequencies and associated vectorial mode profiles of the cavity.

Although, **E**-field, **H**-field and mixed **E**+**H** field formulations have been proposed [19], here we have considered the **H**-field based formulation which shows great advantages [16]-[18], [20] regarding natural implementation of the boundary conditions at the dielectric interfaces compared to other formulations. The natural boundaries associated with the formulation is that of a perfect electric walls (PEW), so that the arbitrary conducting guiding walls can be left free. Besides, the chosen **H**-field is continuous at the dielectric interfaces which is convenient for dielectric resonator problems. Considering the advantage of the structural symmetry, when available, the necessary boundary conditions can also be imposed on the boundary interfaces which increases the accuracy and also decreases the computational cost.

The full vectorial **H**-field based 3D-FEM starts from Maxwell's two curl equations. The solution region or the device is discretized into a number of small unstructured volumetric domain, called *elements*. We used first order tetrahedral elements for computational simplicity. Firstly, the **H**-field within each element is calculated and then interrelation of the field distributions in other elements are followed such that the field becomes continuous across the inter-element boundaries. The **H**-field for a single element can be derived from the total sum of the product of shape function vector and field value at each node of the element. As the variational formulation consists of Maxwell's two curl equations, hence their Euler equation follow the Helmholtz's equation but do not necessarily satisfy the divergence equation ( $\text{div. } \mathbf{B} = 0$ ). This causes the presence of spurious solutions spread all over the eigenvalue spectrum along with the real physical modes. Like the 2D-FEM, the appearance of spurious modes are also true for a 3D-FEM. To avoid the presence of spurious solutions, we followed the similar penalty method as reported earlier [17]. We introduced an additional functional with a weighting factor for the penalty number  $\alpha$  in the full vectorial **H**-field formulation. The Euler equation of the modified functional ( $J_e$ ) satisfy the Maxwell's divergence equation ( $\text{div. } \mathbf{B} = 0$ ).

$$J_e = \left[ \int_v (\nabla \times \mathbf{H})^* \cdot \hat{\epsilon}_r^{-1} (\nabla \times \mathbf{H}) dv + \alpha \int_v (\nabla \cdot \mathbf{H})^* (\nabla \cdot \mathbf{H}) dv \right] - k_0^2 \left[ \int_v \mathbf{H}^* \cdot \hat{\mu}_r \mathbf{H} dv \right] \quad (1)$$

and anisotropic materials, a new full vectorial **H**-field based three dimensional Finite Element Method (3D-FEM) is required. Both the Finite Element (FE) formulations (2D and 3D) are based on a variational formulation which is comprehensive to solve complex waveguide and resonator problems with isotropic, anisotropic homogeneous and inhomogeneous media. For 2D waveguide problems,

Here the functional  $J_e$  describes the numerical errors that occurs due to unstructured discretization,  $k_0^2$  denotes the eigenvalue,  $\hat{\epsilon}_r$  and  $\hat{\mu}_r$  are the relative permittivity and permeability tensor of the medium, respectively. By minimizing the functional in the equation (1) by  $\frac{\partial}{\partial \{H\}_e} J_e = 0$ , the overall numerical error is minimized and the compact form of the eigenvalue equation becomes

$$k_0^2 = \left(\frac{\omega}{c}\right)^2 = \frac{\int_v (\nabla \times \mathbf{H})^* \cdot \epsilon_r^{-1} (\nabla \times \mathbf{H}) dv + \alpha \int_v (\nabla \cdot \mathbf{H})^* (\nabla \cdot \mathbf{H}) dv}{\int_v \mathbf{H}^* \cdot \mu_r \mathbf{H} dv} \quad (2)$$

Here  $k_0$  is the wavenumber,  $\omega$  is the angular frequency. The equation (2) is the modified form of often quoted Berk's formulation [19]. The eigenvector corresponding to the eigenvalue shows the quasi-TE and TM mode profiles inside the resonator cavity.

### III. DEVICE GEOMETRY

Schematic structure of our proposed device is shown in Fig. 1. The main device which is of our interest consists of two silicon cores separated by a narrow slot region shown by dashed red box. The compact vertically slotted straight resonating structure is coupled with two in and out integrated bus waveguides. Light from a tunable laser source travels through one bus waveguide and excites the slotted structure at a particular wavelength. Corresponding resonating wavelength ( $\lambda_{\text{res}}$ ) can be picked by the three output facets of the in/out bus waveguides. During the resonance, electromagnetic energy builds up in the slot cavity and the resonance wavelength can be detected from the both facets of output bus waveguide ( $\lambda_{\text{out1}}$  and  $\lambda_{\text{out2}}$ ) and also at the opposite end of the input bus waveguide. The response from the output integrated waveguide is detected by the photodetectors. The silicon slot guide is separated by a silicon dioxide ( $\text{SiO}_2$ ) buffer layer from the silicon substrate. The silicon and silicon dioxide refractive indices are taken as  $n_{\text{Si}} = 3.476$  and  $n_{\text{SiO}_2} = 1.44$ , respectively at the 1550 nm operating wavelength. The key noticeable advantages of the proposed device can be explained in three steps. First, the compact design of the

device due to nano-scale dimensions results high scale integration and ease of fabrication than other complex devices. Second, the slotted resonating structure has a significant advantage over the conventional rib and nano-wire structures. The dominant  $E_x$  field of the quasi-transverse-electric (TE) mode increases inside the slot region which allows a strong light-analyte interaction rather than to use only the evanescent field tail for sensing. Third, a much improved performance e.g. sensitivity (S) and detection limit (DL) can be achievable with the help of first two points. The slot and the surrounded region can be filled with any low-refractive-index, non-linear and organic material of one's interest. Here the efficiency of the proposed device is presented by using the low-indexed sucrose solution in the slot and cover medium which represents the 3D slotted resonating structure as a chemical sensor. We have also characterized the device as a bio-sensor dipped into water, where a 5 nm ultra-thin ( $T_s$ ) bio-layer with refractive index 1.45 has been considered. The fabrication process of our CMOS compatible proposed device without a curved section can be simple compared to other alternative photonic sensing devices. Silicon vertically-slotted structure can easily be fabricated by etching two straight Si rails into a commercially available SOI wafer. Besides, if required further growth of top Si layer on  $\text{SiO}_2$  buffer layer can be achieved by the plasma enhanced chemical vapor deposition (PECVD). The height of the Si layer can be adjusted by precise controlling the growing time or by reducing it. A photoresist thin film is deposited on the Si layer for patterning. Then

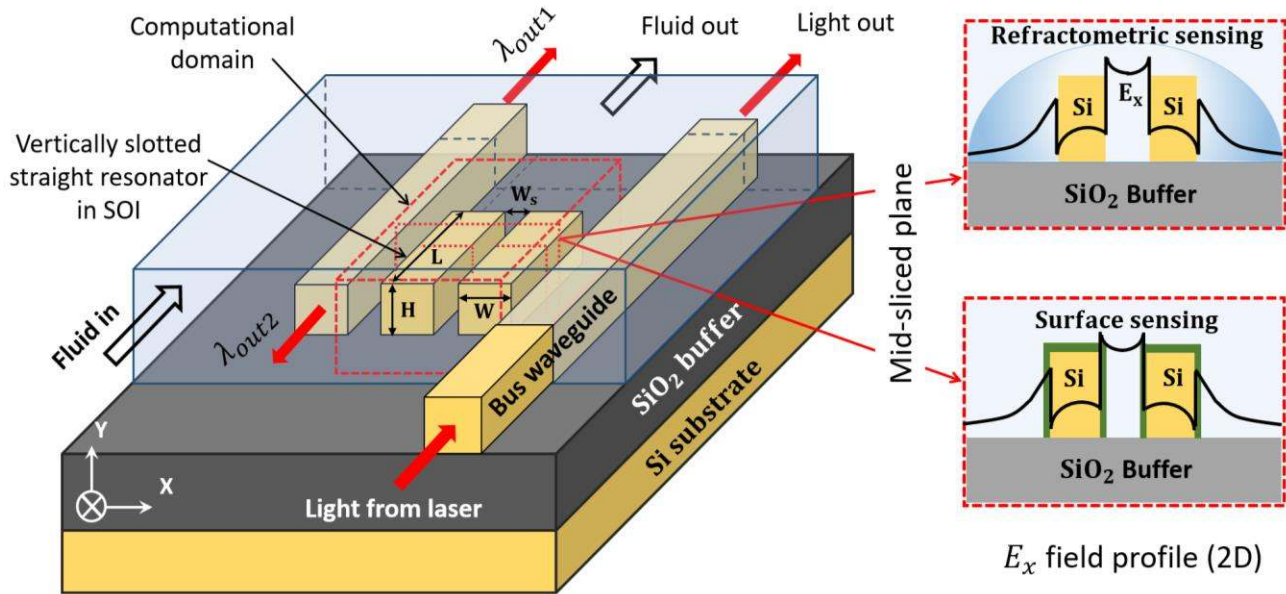


Fig. 1. Three dimensional schematic diagram of single vertically-slotted straight resonator. Red dashed box is showing the computational domain. Insets are showing the mid-sliced plane with dominant  $E_x$  field profile along x-axis shown by black lines.

reactive ion-etching (RIE) is used to make the both Si strips with a slot region in between them.

The rigorous investigation of design parameters, calculation of dominant and non-dominant field components and profiles for the fundamental quasi-TE and TM modes, due to the presence of sensing material with different refractive index values, are of great importance when designing a sensing device. Our in-house two dimensional (2D) [16]-[18] and newly developed three dimensional (3D) Finite Element Method (FEM) are used as numerical tools to obtain the modal solutions of the Si slotted resonator. The 3D slotted resonator is a short length of straight vertical slot waveguide. As a result, a part of the design parameters can be estimated by using the computationally efficient fully vectorial rigorous 2D-FEM.

A 5 nm sensing layer ( $T_s$ ) over the Si core and also inside the slot region is considered for bio-molecule detection, as shown in Fig. 1 bottom inset. The Si core width ( $W$ ), slot height ( $H$ ) and slot width ( $W_s$ ) are optimized for different parameters, such as the power confinements into low-indexed slot and 5 nm sensing bio-layer into the slot region, normalized power density (NPD) and effective index ( $\Delta n_{eff}$ ) change. The  $\Delta n_{eff}$  is the change in the effective index ( $n_{eff}$ ) due to the presence of 5 nm molecular bio-ad layer.

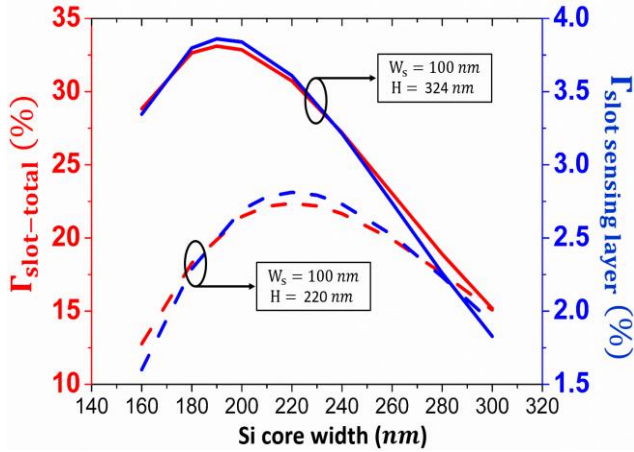


Fig. 2. Optimization of Si core width ( $W$ ) depending on confinement factor ( $\Gamma$ ). Total slot confinement ( $\Gamma_{slot-total}$ ) and confinement of 5 nm sensing layer into slot versus Si core width (nm) for a fixed Si core/slot height of 220 nm and 324 nm. Slot width ( $W_s$ ) is 100 nm. The cover medium, slot region and the sensing layer into slot are filled with water.

Figure 2 shows variation of the power confinement in the slot ( $\Gamma_{slot-total}$ ) and 5 nm sensing layer ( $\Gamma_{slot\ sensing\ layer}$ ) with the Si core width ( $W$ ) by red and blue lines, respectively. The solid and dashed lines show the power confinement variations for two different sets of Si core heights,  $H = 220$  nm and 324 nm, respectively. For both the cases, the slot width ( $W_s$ ) is constant,  $W_s = 100$  nm. When the core is wide enough, the power confinement into Si core is large and this in turn results a low confinement into slot region. It can be observed that with the reduction of the core width ( $W$ ), the confinements increase in the slot and reach their maximum

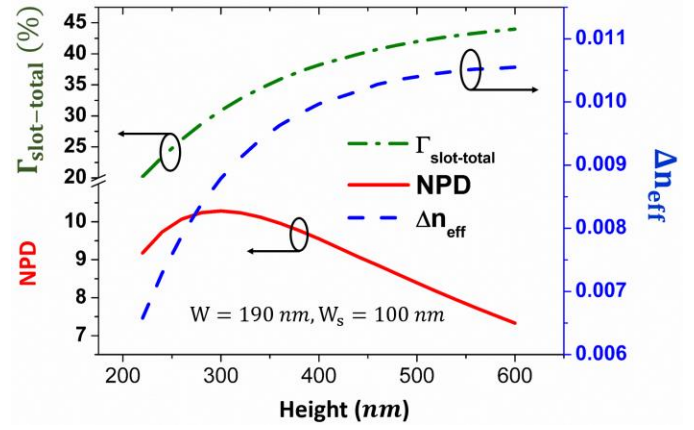


Fig. 3. Optimization of slot height ( $H$ ) depending on confinement factor ( $\Gamma$ ), normalized power density (NPD) and  $\Delta n_{eff}$ . The green dashed-dotted, blue dashed and red solid lines are showing the variation of total slot confinement ( $\Gamma_{slot-total}$ ),  $\Delta n_{eff}$  and normalized power density (NPD) with slot height ( $H$ ). The Si core width ( $W$ ) and slot width ( $W_s$ ) are kept fixed at 190 nm and 100 nm. The cover medium, slot region and the sensing layer into slot are filled with water.

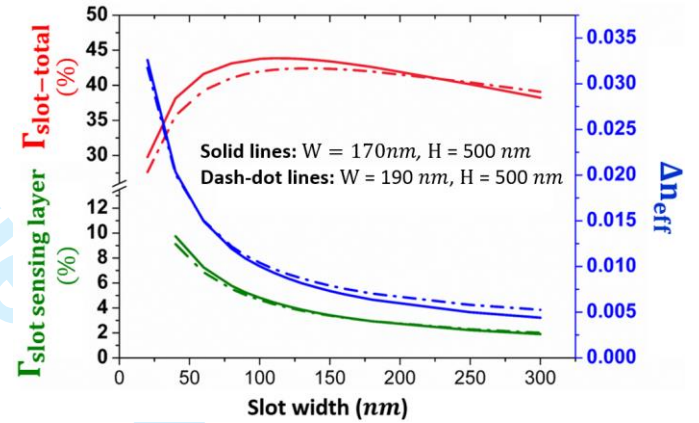


Fig. 4. Optimization of slot width ( $W_s$ ). The solid lines (red, green and blue) illustrates the variation of  $\Gamma_{slot-total}$ ,  $\Gamma_{slot\ sensing\ layer}$  and  $\Delta n_{eff}$  with  $W_s$  for  $W = 170$  nm and  $H = 500$  nm and the dashed-dotted lines (red, green and blue) depicts the same for 190 nm Si strip width ( $W$ ) and 500 nm height ( $H$ ).

values at  $W = 190$  nm and  $W = 220$  nm for  $H = 324$  nm and  $H = 220$  nm, respectively. Subsequently a rapid fall of confinement in slot region is also noticeable with the further reduction of  $W$ . The power confinement of sensing layer into slot region ( $\Gamma_{slot\ sensing\ layer}$ ) also shows similar trend as that of  $\Gamma_{slot-total}$ . To study the effect of core height, the variations of total slot confinement ( $\Gamma_{slot-total}$ ), normalized power density (NPD) in the slot and change of effective index ( $\Delta n_{eff}$ ) with slot or Si core height ( $H$ ) are shown in Fig. 3. Here the partially optimized core width ( $W$ ) is taken as 190 nm and slot width as 100 nm. The green dashed-dot line shows the increase of total power confinement into slot region ( $\Gamma_{slot-total}$ ) with the  $H$ . Normalized power density (NPD) is another important design parameter in sensing device optimization, when especially the localized high power density is exploited, such as an ultra-thin bio or chemical layer in the slot region. The variation of normalized power density (NPD), shown by a red solid curve, which initially increases

as slot height (H) increases and reaches a maximum value at  $H = 300 \text{ nm}$ . But with the further increment of H, the normalized power density (NPD) decreases. Here the variation of effective index shift ( $\Delta n_{eff}$ ) due to the presence of  $5 \text{ nm}$  thick molecular bio-ad layer with H is a key design parameter and shown by a blue dashed line. The variation of  $\Delta n_{eff}$  with the H shows a strong correlation with the  $\Gamma_{slot-total}$  variation. Both the parameters increase, as the slot height (H) increases. Although, generally SOI structures with  $H = 220 \text{ nm}$  is more widely used, however, as it is shown here that higher heights yield better sensors, so optimized slot height for our device is taken as  $500 \text{ nm}$ , which would be easy to fabricate [21], yields  $\Gamma_{slot-total} = 41.965\%$  and  $\Delta n_{eff} = 0.0104$ .

So far we have kept the slot width ( $W_s$ ) fixed at  $100 \text{ nm}$ , as it was theoretically optimized for slot waveguide based homogeneous sensor [22] and also successfully used in label-free slot based ring resonator for bio sensing application [5]. However, the slot width ( $W_s$ ) variation with optimized W ( $190 \text{ nm}$ ) and H ( $500 \text{ nm}$ ) shows the maximum  $\Gamma_{slot-total} = 42.405\%$  at a slightly wider slot width,  $W_s = 130 \text{ nm}$ , shown by a red dashed-dotted line in Fig. 4. Here the confinement of sensing layer into slot ( $\Gamma_{slot \text{ sensing layer}}$ ) with green dashed-dotted line and effective index change ( $\Delta n_{eff}$ ) with blue dashed-dotted line shows a strong correlation and both of them decrease with the increment of slot width ( $W_s$ ). As a very small slot width may not easy to fabricate, hence total confinement into slot ( $\Gamma_{slot-total}$ ) can be taken as a critical factor. A further investigation of  $\Gamma_{slot-total}$  variation with W by keeping  $W_s$  and H fixed at  $130 \text{ nm}$  and  $500 \text{ nm}$ , respectively, gives only a small change in earlier optimized W and shows maximum confinement ( $\Gamma_{slot-total} = 43.751\%$ ) at  $W = 170 \text{ nm}$ . The red, green and blue solid lines in Fig. 4 shows the  $\Gamma_{slot-total}$ ,  $\Gamma_{slot \text{ sensing layer}}$  and  $\Delta n_{eff}$  variations with slot width ( $W_s$ ), for  $W = 170 \text{ nm}$  and this set suggests a new value,  $W_s = 110 \text{ nm}$  when  $\Gamma_{slot-total}$  becomes maximum. As there was not much difference in  $\Gamma_{slot-total}$  for  $W = 170$  and  $190 \text{ nm}$  and a few  $\text{nm}$  extra slot width which may also be convenient for fabrication, we have finalized the optimized slot width as  $130 \text{ nm}$ . Hence all the optimized 2D design parameters of slot structure can be taken as,  $W = 170 \text{ nm}$ ,  $H = 500 \text{ nm}$  and  $W_s = 130 \text{ nm}$  when the cover medium and the slot region is considered to be filled up with aqueous solution of refractive index 1.33. The full vectorial 2D-FEM has again been applied to determine the effective index ( $n_{eff}$ ) of the optimized structure and this value is 1.63827. The corresponding 2D  $E_x$  field profile is shown in Fig. 5. Throughout these 2D-FEM simulations, the structure is discretized with 1,280,000 first order triangular elements.

Next, we design the vertically slotted resonating structure using the optimized W, H and  $W_s$  (Fig. 1) discussed above. The slot supports longitudinal modes that resonance at a specific wavelength ( $\lambda_{res}$ ) as,

$$\lambda_{res} = \frac{2L.n_{eff}}{m} \quad (3)$$

Here  $m$  is the longitudinal mode order inside the cavity

( $m = 1, 2, 3 \dots$ ) and  $2L$  denotes the round trip length of the electromagnetic wave in the resonator. As the fundamental mode is expected to be more stable and sensitive than other higher order modes, we calculate the length (L) of the slot resonator using equation (3) for the fundamental mode ( $m = 1$ ). Finally, all the device dimensions have been considered can be summarized as, Si core width ( $W$ ) =  $170 \text{ nm}$ , slot height ( $H$ ) =  $500 \text{ nm}$ , slot width ( $W_s$ ) =  $130 \text{ nm}$  and the device length ( $L$ ) =  $473.06 \text{ nm}$  for the expected resonating wavelength ( $\lambda$ ) of  $1550 \text{ nm}$ .

In and out straight bus waveguides can be used to connect the resonator cavity with the light source and detectors. A phase matched Si strip waveguide of width  $218 \text{ nm}$  and height  $500 \text{ nm}$  can be used as bus, shown in Fig. 1. The gap between resonator and adjacent bus waveguide can be within the range of  $250 \text{ nm}$  to  $400 \text{ nm}$  to achieve a good coupling. Alternatively, to maintain the phase matched condition, a slot waveguide having the same dimensions:  $W = 170 \text{ nm}$ ,  $H = 500 \text{ nm}$  and  $W_s = 130 \text{ nm}$  can also be used as bus waveguide. Here a  $300$  to  $400 \text{ nm}$  gap can be useful to couple light wave in between resonator and in/out bus waveguide.

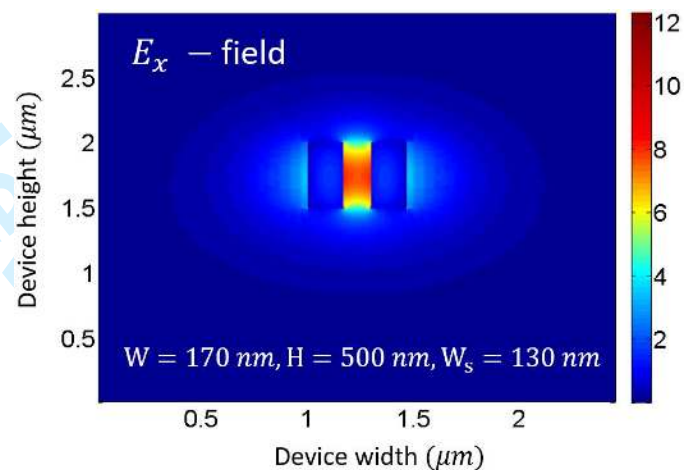


Fig. 5. Enhanced  $E_x$  field into slot region for optimized device dimensions: Si strip width ( $W$ ) =  $170 \text{ nm}$ , height ( $H$ ) =  $500 \text{ nm}$  and  $W_s = 130 \text{ nm}$ . 2D-FEM code is used for simulation.

#### IV. PERFORMANCE ANALYSIS

In a resonating structure the self-consistent field gets confined and oscillates at a particular frequency, hence the basic performance investigation requires complete three dimensional field analysis of the quasi-TE and TM modes inside the resonating structure. For the present work, a dedicated rigorous and full vectorial  $\mathbf{H}$ -field based three dimensional finite element (3D-FEM) code is developed to solve the problem. We divided the performance analysis into two stages: (1) surface sensing with an ultra-thin bio-molecular layer covers the sensor surface (see Fig. 1, bottom inset) and (2) homogeneous refractometric sensing (see Fig. 1, top inset), where sensitivity for bulk refractive index change in surrounding medium is considered.

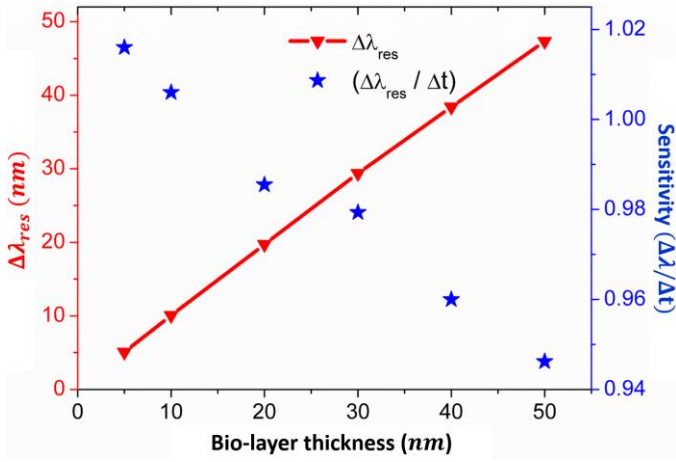


Fig. 6. Surface sensing of the proposed device with optimized design parameters. The red line depicts a linear resonance wavelength shift ( $\Delta\lambda_{res}$ ) for different bio-layer thickness of refractive index 1.45. The blue stars denote the surface sensitivity ( $S_{surface}$ ) variation with bio-layer thickness ranging from 5 nm to 50 nm.

#### A. Surface Sensing

The first stage of our investigation is based on homogeneous bio-sensing where we have considered a thick bio-ad layer (refractive index 1.45) on both the Si strips and inside the slot region. The cover medium is filled with aqueous solution ( $n_{water} = 1.33$ ). For detail analysis we have also considered different thickness of sensing layers ranging from 5 nm to 50 nm. During the 3D-FEM simulations, we have verified the numerical accuracy by considering over 456817 first order tetrahedral elements in the computational domain of  $1.47 \mu m$  (along x)  $\times$   $0.47306 \mu m$  (along y)  $\times$   $1.5 \mu m$  (along z). A resonating wavelength shift from 1537.21 nm to 1542.38 nm was observed due to the presence of ultra-thin 5 nm sensing layer with refractive index of 1.45. Hence the refractive index change in the sensing layer causes a resonance shift ( $\Delta\lambda_{res}$ ) of 5.2 nm for surface sensing. We have also studied the surface sensitivity ( $S_{surface}$ ) for different bio-layer thickness. The  $\Delta\lambda_{res}$  linearly increases with the thickness of sensing layer. This is shown by a red solid line in Fig. 6, depict a strong linear resonance shift ( $\Delta\lambda_{res}$ ) with bio-layer thickness change ( $\Delta t$ ). The blue stars denote the variation of surface sensitivity  $S_{surface} = (\Delta\lambda_{res}/\Delta t)$  against different bio-layer thickness, plotted in a high resolution scale. A small reduction of  $S_{surface}$  can be observed with the increment bio-layer thickness. Our simulation shows almost similar sensitivity as reported in [5] but in our case with a simpler straight structure.

#### B. Bulk Refractive Index Sensing

The second stage of sensitivity investigation follows the detection of bulk refractive index change in the cover and the slot region. Aqueous sucrose solutions with different concentrations are used over the sensing device. The refractive index of sucrose-water solution for different sucrose concentration at ambient temperature (20°C) are taken from

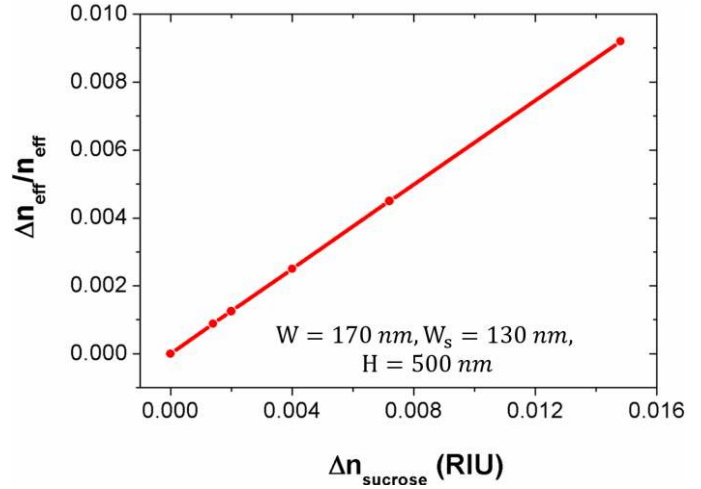


Fig. 7. Bulk refractometric sensitivity ( $S$ ) analysis of vertically single slotted waveguide with optimized design parameters at 1550 nm. The slope of the curve denotes the sensitivity of the slot waveguide while the cover medium is filled with sucrose solution.

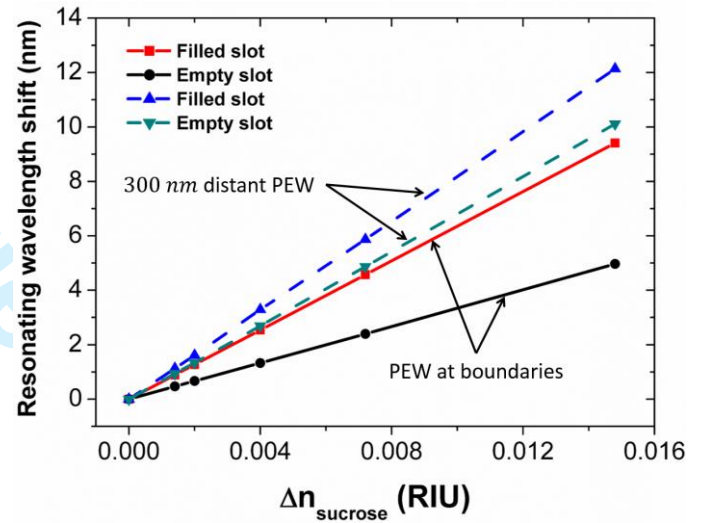


Fig. 8. Bulk sensitivity ( $S_{bulk}$ ) analysis of the proposed device. Resonating wavelength shift (nm) versus refractive index variation ( $\Delta n_{sucrose}$ ) of sucrose solution at ambient temperature (20°C). The solid lines illustrate the resonating wavelength shift when the perfect electric walls (PEW) are touching the end faces of Si core. The dashed lines present the same when the PEWs are 300 nm away from both end faces of the Si core. The slope of each linear curve represents the sensitivity ( $S_{bulk}$ ) for the filled and empty conditions.

[23]. Two different cases are considered during simulation process: (1) the slot region and cover medium are completely filled with the fluid, and (2) only cover medium is filled with sucrose solution and the narrow slot region is filled with air bubble. In the present formulation, the natural boundary condition is that of a perfect electric wall (PEW). If the structure is enclosed inside a metal box, then we do not need to impose the boundary condition. However, for an open type resonating structure, the computational boundary should be away from the resonating structure. The bulk sensitivity ( $S_{bulk}$ ) also depends on the position of computational or physical electric wall. Figure 7 depicts the bulk refractive

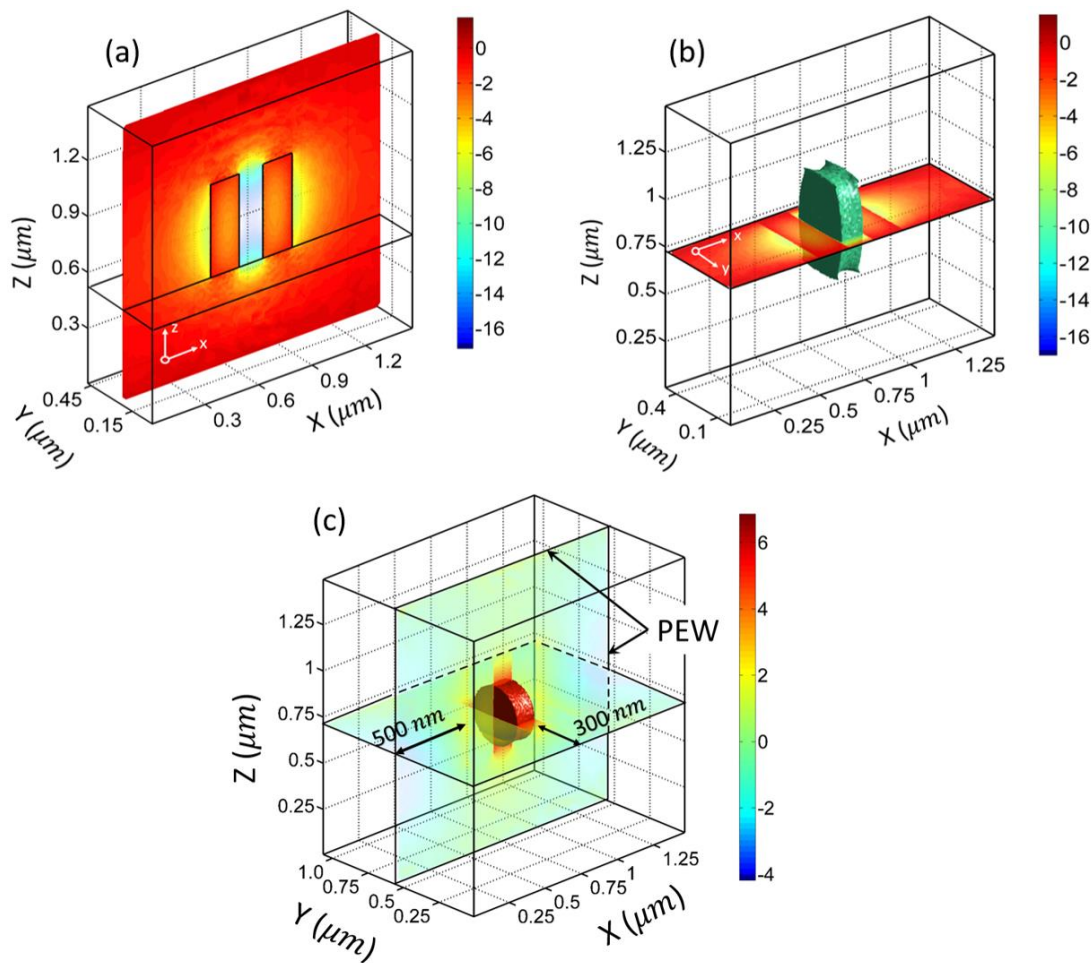


Fig. 9. The dominant  $E_x$  field (2D and 3D) confined into straight single slotted resonator with optimized design parameters at the telecommunication wavelength. Field profiles are generated by post-processing of eigenvectors of resonating wavelength ( $\lambda_{res}$  being an eigenvalue), (a) shows the  $E_x$  field profile of slot resonator on an x-z sliced plane and (b) depicts the 3D iso-surface profile of  $E_x$  field. The PEWs are considered at both end faces of the Si cores. (c) 3D iso-surface profile of confined  $E_x$  field when the boundary PEWs are 300 nm and 500 nm away from both end faces and side faces of Si strips, respectively. Full vectorial 3D-FEM is used for complete resonating structure simulation.

index sensitivity of the optimized single vertically-slotted waveguide simulated by 2D-FEM. The variation of normalized effective index change ( $\Delta n_{eff}/n_{eff}$ ) with different refractive indices of sucrose solution is presented by the red solid line. The slope gives us the sensitivity  $S_{bulk} = (\Delta n_{eff}/n_{eff})/RIU$  of 1.025 per RIU. Figure 8 shows the resonance wavelength shift ( $\Delta\lambda$ ) of the resonating structure as a function of refractive index of sucrose solution at 20°C. The solid line shows the variation of resonance wavelength shift ( $\Delta\lambda$ ) with the change of refractive index of sucrose solution when the PEWs are placed at both end faces of Si strips. A strong linear shift is observed, and the slope of the lines i.e. sensitivity ( $S_{bulk}$ ) shows the value of 635 nm/RIU and 335 nm/RIU for the fully filled and for the case of empty slot (a case arises when sensing liquid may not enter the slot region), respectively. A significant improvement can be observed of the proposed device sensitivity compared to the other devices reported earlier [3]-[10]. The dashed line also shows a linear shift of resonance wavelength ( $\Delta\lambda$ ) when the PEWs are positioned at 300 nm away from both the end faces of the Si core strips. Corresponding 3D iso-surface profiles of confined

$E_x$  fields for both cases are shown in Fig. 9. The 3D iso-surface field profiles are generated by the post-processing of the eigenvectors obtained from complete device simulation by the developed 3D-FEM. Fluid-Si surface contact increases when the boundary walls are kept away from the Si strip's end faces. As a result, a greater sensitivity has been observed, illustrated by the blue and the green dashed lines with slope 820 nm/RIU and 683 nm/RIU for filled and empty slot region, respectively. These values are much higher and shows a considerable improvement over the theoretically and experimentally investigated sensing devices reported so far [3]-[10]. Besides the spectral shift i.e. sensitivity, detection limit (DL) is another important parameter to illustrate the efficiency of the sensor to detect and quantify the properties of the deposited sample of interest. The DL can be estimated from the sensitivity ( $S_{bulk}$ ) and the sensor resolution (R) as,  $DL = R/S_{bulk}$ . The resolution of the device is controlled by the wavelength resolution ( $\lambda_{resolution}$ ) of the light source and sensitivity ( $S_{bulk}$ ) is the slope of the curves in Fig. 8. If we consider a laser source having wavelength resolution of 5 pm [6], a minimal detectable refractive index of  $7.9 \times 10^{-6}$  RIU

and  $6.1 \times 10^{-6}$  RIU could be achieved for PEW touching the facets and 300 nm away from the Si strip facets, respectively.

## V. FABRICATION TOLERANCE STUDY

To achieve a robust device design, it is important to study the effect of fabrication tolerances. We have analyzed three important design parameters such as, total slot confinement ( $\Gamma_{\text{slot-total}}$ ), surface sensitivity ( $S_{\text{surface}}$ ) and bulk sensitivity ( $S_{\text{bulk}}$ ) with the device parameters by changing a few % of the optimized Si core width (W), slot height (H) and slot width ( $W_s$ ).  $S_{\text{surface}}$  and  $S_{\text{bulk}}$  are studied for 5 nm bio-ad layer and 5% sucrose solution over the device. We found  $\Gamma_{\text{slot-total}} > 43\%$  for variation in W from -5% to +8% in the case of ideal situation (cover and slot region are filled with aqueous solution). During the growth of Si core, it may not always be possible to maintain the optimum slot height and slot width. Our study shows a considerable  $\Gamma_{\text{slot-total}}$  variation from 40.96% to 45.91% with H variation within  $\pm 10\%$ . Besides, for the same variation of slot width ( $W_s$ ),  $\Gamma_{\text{slot-total}}$  remains  $> 43\%$ . In terms of sensitivity analysis,  $S_{\text{surface}}$  varies from -5.39% to +3.92% for W variation within  $\pm 6\%$ . We also obtained -1.59% to +1.47% and +4.16% to -3.67%  $S_{\text{surface}}$  variation for the change in H and  $W_s$  within  $\pm 5\%$ . On the other hand, bulk sensitivity ( $S_{\text{bulk}}$ ) shows a much smaller -3.12% to 0.40% change for -10% to +5% variation of W. Similarly, the variation of H and  $W_s$  within  $\pm 10\%$  results a small acceptable variation in  $S_{\text{bulk}}$  from -2.44% to +1.63% and +0.67% to -0.77%, respectively. These results indicate that the device can achieve over 43% total slot confinement and only smaller sensitivity change with  $\pm 5\%$  fabrication imperfections. Thus, our proposed resonating structure is robust and possible to fabricate with the available CMOS fabrication technology.

## VI. CONCLUSION

We report a SOI based, single vertically-slotted resonator as an efficient biochemical sensor, which will be easy to fabricate. Device performance has been studied for surface sensing with a 5 nm bio-ad layer and bulk refractive index changes in the cover and slot region. A rigorous full vectorial 3D-FEM is developed and used to simulate the device for different sensing applications. We obtain a record sensitivity of 5.2 nm resonance wavelength shift for surface sensing. On the other hand, an improved linear resonating wavelength shift of 635 nm/RIU and 820 nm/RIU have been achieved for homogeneous refractometric sensing. The detection limit as low as  $6.1 \times 10^{-6}$  RIU can be achieved.

Typical waveguide loss for vertical slots have been measured as  $< 20$  dB/cm [24]. However, water also absorbs light at 1550 nm and this value has been given as 47.5 dB/cm [5]. In our design, nearly 20% of the power is confined in the water cladding, similar as reported in [5]. So for the vertical slotted resonator shorter than 1  $\mu\text{m}$ , as reported here, the propagation loss of the slotted structure will be very small and neglected in our simulations. A rigorous least-squares boundary residual (LSBR) method is used to calculate the power transfer, the back reflection coefficient ( $\rho_r$ ) and transmission loss of the butt coupled strip waveguide and slotted resonator for different gaps. For three different gaps

250, 300 and 400 nm, the power transfer from strip to slot resonator are 1.67%, 1.12% and 0.512%, respectively. Some input signals also reflected from the junction between the input guide and the resonator section with slot guide and these reflection coefficients ( $\rho_r$ ) have been calculated as 0.024, 0.020 and 0.012, for separations 250 nm, 300 nm and 400 nm, respectively. On the other hand, the coupling losses at this junction are also calculated by using the LSBR method. These coupling losses are 0.2886 dB, 0.1956 dB and 0.0833 dB for separations 250 nm, 300 nm and 400 nm, respectively. It can be noted that 250 nm gap provides higher evanescent coupling to slot waveguides but with also higher butt-coupling loss from the input guide, whereas the 400 nm gap provides less evanescent coupling but with a higher butt-coupling efficiency. Thus a suitable separation could be in the range of 250 to 400 nm.

Our proposal serves the successful demonstration of label-free bio-chemical sensing applications of low-index confined electromagnetic field in a slotted Fabry-Perot resonating structure by using a full-vectorial 3D-FEM code. This nano-structural geometry is relatively simple and compact compared to other complex photonic devices such as slotted ring resonator and nano-Bragg grating sensors. This can be realized in practice with the help of well-matured state-of-the-art fabrication technologies and surface chemistry [21], [24], [25]. Based on the preliminary results this slot resonator device shows a great potential to be employed as bio-chemical sensor.

## ACKNOWLEDGMENT

This work was supported by City University London. The authors thank Erasmus Mundus Areas+ PhD fellowship program for PhD and research funding.

## REFERENCES

- [1] R. A. Soref and J. P. Lorenzo, "All-silicon active and passive guided-wave components for  $\lambda = 1.3$  and  $1.6 \mu\text{m}$ ," *IEEE J. Quantum Electronics*, vol. 3, no. 22, pp. 873 – 879, Jun. 1986.
- [2] V. R. Almeida, Q. Xu, C. A. Barrios and M. Lipson, "Guiding and confining light in void nanostructure," *Opt. Lett.*, vol. 29, no. 11, pp. 1209 – 1211, Jun. 2004.
- [3] C. A. Barrios, K. B. Gylfason, B. Sanchez, A. Griol, H. Sohlstrom, M. Holgado and R. Casquel, "Slot-waveguide biochemical sensor," *Opt. Lett.*, vol. 32, no. 21, pp. 3080 – 3082, Nov. 2007.
- [4] C. A. Barrios, M. J. Banuls, V. Gonzalez-Pedro, K. B. Gylfason, B. Sanchez, A. Griol, A. Maquieira, H. Sohlstrom, M. Holgado and R. Casquel, "Label-free optical biosensing with slot-waveguides," *Opt. Lett.*, vol. 33, no. 7, pp. 708 – 710, 2008.
- [5] T. Claes, J. G. Molera, K. D. Vos, E. Schacht, R. Baets, and P. Bienstman, "Label-free biosensing with a slot-waveguide based ring resonator in silicon on insulator," *IEEE Photon. J.*, vol. 1, no. 3, pp. 197 – 204, 2009.
- [6] K. D. Vos, I. Bartolozzi, E. Schacht, P. Bienstman and R. Baets, "Silicon-on-insulator microring resonator for sensitive and label-free biosensing," *Opt. Express*, vol. 15, no. 12, pp. 7610 – 7615, 2007.
- [7] S. T. Fard, S. M. Grist, V. Donzella, S. A. Schmidt, J. Flueckiger, W. Shi, A. Millspugh, M. Webb, D. M. Ratner, K. C. Cheung and L. Chrostowski, "Label-free silicon photonic biosensors for use in clinical diagnostics," in *Proc. SPIE 8629*, 862909, 2013.
- [8] A. S. Jugessur, J. Dou, J. S. Aitchison, R. M. De La Rue and M. Gnan, "A photonic nano-Bragg grating device integrated with microfluidic channels for bio-sensing applications," *Microelectron. Eng.*, vol. 86, no. 4-6, pp. 1488 – 1490, Jun. 2009.

- [9] X. Wang, S. Grist, J. Flueckiger, N. A. F. Jaeger and L. Chrostowski, "Silicon photonic slot waveguide Bragg gratings and resonators," *Opt. Express*, vol. 21, no. 16, pp. 19029 – 19039, 2013.
- [10] G. A. Rodriguez, S. Hu and S. M. Weiss, "Porous silicon ring resonator for compact, high sensitivity biosensing applications," *Opt. Express*, vol. 23, no. 6, pp. 7111 – 7119, 2015.
- [11] T. Lipka, L. Wahn, H. K. Trieu, L. Hilterhaus and J. Muller, "Label-free photonic biosensors fabricated with low-loss hydrogenated amorphous silicon resonators," *J. Nanophoton*, vol. 7, no. 1, pp. 073793, 2013.
- [12] C. Caer, S. F. Serna-Otalvaro, W. Zhang, X. L. Roux and E. Cassan, "Liquid sensor based on high-Q slot photonic crystal cavity in silicon-on-insulator configuration," *Opt. Lett.*, vol. 39, no. 20, pp. 5792 – 5794, 2014.
- [13] D. Yang, C. Wang and Y. Ji, "Silicon on-chip 1D photonic crystal nanobeam bandstop filters for the parallel multiplexing of ultra-compact integrated sensor array," *Opt. Express*, vol. 24, no. 15, pp. 16267 – 16279, 2016.
- [14] B. J. Luff, J. S. Wilkinson, J. Piehler, U. Hollenbach, J. Ingenhoff and N. Fabricius, "Integrated optical Mach-Zehnder biosensor," *J. Lightwave Technol.*, vol. 16, no. 4, pp. 583 – 592, 1998.
- [15] K. Misiakos, I. Raptis, A. Salapatas, E. Makarona, A. Botsialas, M. Hoekman, R. Stoffer and G. Jobst, "Broad-band Mach-Zehnder interferometers as high performance refractive index sensors: Theory and monolithic implementation," *Opt. Express*, vol. 22, no. 8, pp. 8856 – 8870, 2014.
- [16] B. M. A. Rahman and J. B. Davies, "Finite-element solution of integrated optical waveguides," *J. Lightwave Technol.*, vol. 2, no. 5, pp. 682 – 688, Oct. 1984.
- [17] B. M. A. Rahman and J. B. Davies, "Penalty function improvement of waveguide solution by finite element," *IEEE Trans. Microwave Theory Tech.*, vol. 32, no. 8, pp. 922 – 928, Aug. 1984.
- [18] B. M. A. Rahman, "Finite element analysis of optical waveguides," in *Methods for Optical Guided-Wave Devices: Part I, Modes and Couplings*. W. P. Huang, Ed. Cambridge, MA: EMW Publishing, pp. 187 – 216, 1995.
- [19] A. D. Berk, "Variational principles for electromagnetic resonators and waveguides," *IRE Trans. On Antennas and Propagation*, vol. 4, pp. 104 – 111, Apr. 1956.
- [20] J.-M. Jin, "The Finite Element Method in Electromagnetics 3<sup>rd</sup> ed.," Wiley-IEEE press 2014.
- [21] S. H. Yang, M. L. Cooper, P. R. Bandaru and S. Mookherjee, "Giant birefringence in multi-slotted silicon nanophotonic waveguides," *Opt. Express*, vol. 16, no. 11, pp. 8306 – 8316, 2008.
- [22] F. Dell'Olio and V. M. N. Passaro, "Optical sensing by optimized silicon slot waveguides," *Opt. Express*, vol. 15, no. 8, pp. 4977 – 4993, 2007.
- [23] *Sucrose Conversion Table*, FILE CODE 135-A-50, United States Department of Agriculture (USDA), Jan. 1981.
- [24] C. A. Barrios, B. Sanchez, K. B. Gylfason, A. Griol, H. Sohlstrom, M. Holgado and R. Casquel, "Demonstration of slot-waveguide structures on silicon nitride / silicon oxide platform," *Opt. Express*, vol. 15, no. 11, pp. 6846 – 6856, 2007.
- [25] A. Saynatjoki, T. Alasaarela, A. Khanna, L. Karvonen, P. Stenberg, M. Kuittinen, A. Trevenon and S. Honkanen, "Angled sidewalls in silicon slot waveguides: conformal filling and mode properties," *Opt. Express*, vol. 17, no. 23, pp. 21066 – 21076, 2009.

element method for simulation of complex plasmonic waveguides and resonators.

**B. M. A. Rahman** (S'80 - M'83 – SM'94 – F'2016) received his B.Sc Eng. And M.Sc. Eng. Degrees (with distinctions) in Electrical Engineering from the Bangladesh University of Engineering and Technology (BUET), Dhaka, Bangladesh, in 1976 and 1979, respectively, and received two gold medals for being the best undergraduate and graduate students of the university in 1976 and 1979, respectively. In 1979, he received a Commonwealth Scholarship and in 1982 obtained a Ph.D degree in Electronics from University College London, London, U.K.

From 1976 to 1979, he was a Lecturer in the Department of Electrical Engineering, BUET. In 1982, he was a Postdoctoral Research Fellow at University College London. In 1988, he joined City University London, London, U.K., as a Lecturer, where he is now a Professor, and leads the research group on photonics modelling, specialized in the use of rigorous and full-vectorial numerical approaches to design, analyse, and optimize a wide range of photonic devices, such as spot-size converters, high-speed optical modulators, compact bend designs, power splitters, polarization splitters, polarization rotators, polarization controllers, THz devices, etc. He is the author or co-author of more than 500 journal and conference papers, and his journal papers have been cited more than 3500 times. He is a Fellow of the IEEE, Optical Society of America (OSA) and SPIE. He is a Chartered Engineer, U.K.

**Souvik Ghosh** was born in Kolkata, India. He received his B.Tech and M.Tech degree in Optics and Optoelectronics (First class, 1<sup>st</sup> rank) from Calcutta University (C.U), India in 2012 and 2014, respectively. He is currently pursuing Ph.D degree at the School of Mathematics, Computer Science and Engineering, City University London, London, U.K. He is also a recipient of Erasmus Mundus Areas+ Ph.D fellowship.

His research interests include the application of two dimensional and three dimensional finite element method in photonic devices, waveguides as well as resonators. Currently he is working on the development and application of finite